Construction and simulation of filter bubble model of angiosperms pitted membrane

This study focuses on the perforated membrane and establishes a model to verify the mechanism of bubble filtration through the perforated membrane and the influence of pore size on the pressure during bubble leakage using numerical simulation. Due to the complex porous structure inside the perforated membrane, it will be simplified for physical structure, followed by simulation analysis of its bubble filtration process.

The fundamental theory of numerical simulation.

To validate the mechanism of bubble filtration through the perforated membrane, this study conducted simulation and modeling of the bubble filtration process using COMSOL Multiphysics software. COMSOL Multiphysics is a numerical simulation software based on the finite element method, specifically designed to describe and simulate various real physical phenomena.

In the two-phase flow of gas and liquid, the liquid phase is considered as the continuous phase, while the gas phase is regarded as the dispersed phase. The liquid phase is assumed to be incompressible, while the gas phase follows the ideal gas equation. Additionally, surface tension exists at the interface of the bubbles.

The continuity equation for the continuous phase is expressed as:

$$\frac{\partial \rho}{\partial t} + \frac{\partial (\rho u)}{\partial x} + \frac{\partial (\rho v)}{\partial y} + \frac{\partial (\rho w)}{\partial z} = 0$$

Introducing:

$$\nabla \bullet \alpha = \mathrm{div}(\alpha) = \frac{\partial \alpha_x}{\partial x} + \frac{\partial \alpha_y}{\partial y} + \frac{\partial \alpha_z}{\partial z}$$

The continuity equation then becomes:

$$\frac{\partial \rho}{\partial t} + \nabla \cdot (\rho \vec{u}) = 0$$

t represents time, ρ is the density of the continuous phase, $\vec{u}$ is the velocity vector, and u, v, w are the velocity components in the x, y, z directions respectively.

The momentum conservation equation:

$$\frac{\partial (\rho \vec{u})}{\partial t} + \nabla \cdot (\rho \vec{u}\vec{u}) = -\nabla p + \rho g + \nabla \cdot \mu \left(\nabla \vec{u} + \nabla \vec{u}^{\mathrm{T}} \right) + \mathbf{F}_{\sigma}$$

p represents pressure, ρ and μ are the density and viscosity of the continuous phase respectively, g is the gravitational acceleration, and $\mathbf{F}_{\sigma}$ represents surface tension.

The energy equation:

$$\frac{\partial}{\partial t}(\rho E)+\nabla\cdot(\vec{u}(\rho E+p))=\nabla\cdot\left(k_{eff}\nabla T\right)+S_h$$

During simulation with COMSOL Multiphysics, the two-phase flow level set model was selected to track the gas-liquid interface in real time. The two-phase flow level set model can clearly depict the actual flow of the two incompatible fluids. The equation governing the interface change is:

$$\frac{\partial\phi}{\partial t}+\mu\cdot\nabla\phi=\gamma\nabla\left[\varepsilon_{ls}\nabla\phi-\phi(1-\phi)\frac{\nabla\phi}{|\nabla\phi|}\right]$$

ϕ, ε_{ls}, γ and μ represent the level set function, interface thickness, reinitialization quantity, and fluid viscosity respectively. The fluid viscosity and density are:

$$\rho=\rho_{Air}+\left(\rho_{water}-\rho_{Air}\right)\phi$$

$$\mu=\mu_{Air}+\left(\mu_{water}-\mu_{Air}\right)\phi$$

The Navier-Stokes equations applied in the two-phase flow level set model are as follows:

$$\rho\frac{\partial u}{\partial t}+\rho\left(u\cdot\nabla\right)u=F_{\sigma}+\nabla\left[-pl+\mu\left(\nabla u+(\nabla u)^T\right)\right]+\rho g$$

Computational model and mesh generation.

The perforated membrane is a cellulose-based porous medium composed of multiple layers of cellulose microfibrils. As shown in Fig. S1, the perforated membrane consists of multiple layers of microfibril layers arranged in different directions, with the cellulose microfibrils within each layer arranged in parallel.
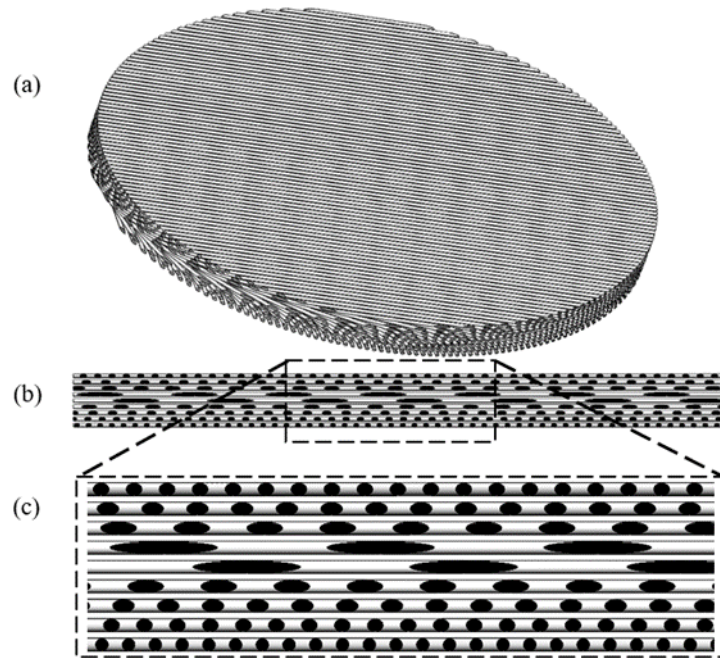

Fig. S1 Three-dimensional structure of pit membrane.

Porous media exhibit characteristics such as the randomness of pore connectivity, the complexity of pore geometry, and the distribution of pore sizes, making direct theoretical analysis challenging and necessitating simplification. Straight channels exhibit one-dimensional connectivity, meandering channels exhibit quasi-two-dimensional connectivity, and porous media exhibit three-dimensional connectivity. In this section, the three-dimensional structure of the perforated membrane is simplified to facilitate the analysis of its gas-liquid two-phase flow behavior. The three-dimensional connectivity model of porous media is simplified to a two-dimensional connectivity model, as shown in Fig. S2, where an interleaved array of micro-columns replaces the three-dimensional porous medium.
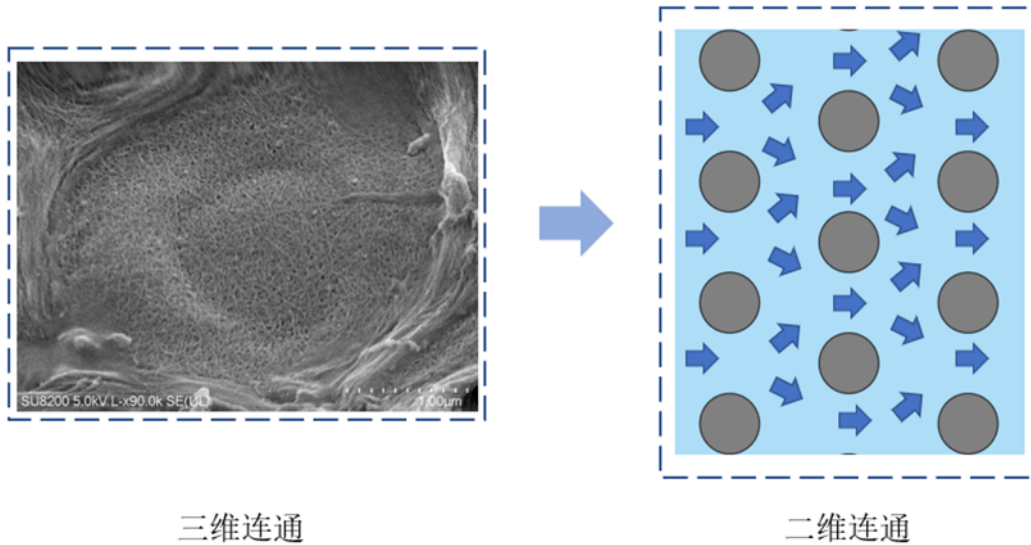

三维连通   二维连通
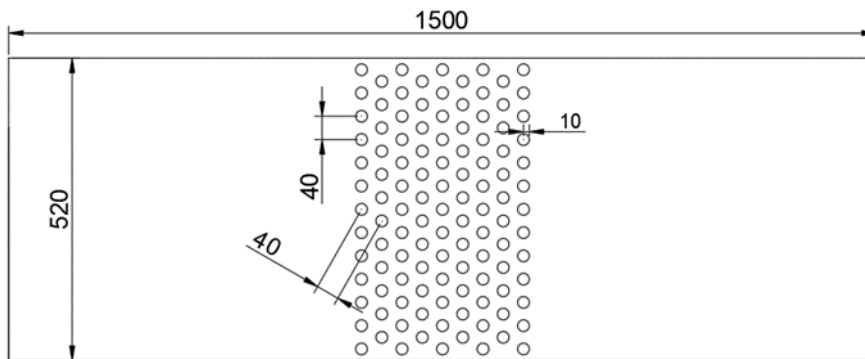
Fig. S2 Simplified model.

Fig. S3 Schematic diagram of the calculation model structure. (unit: nm)

The computational model for simulation using COMSOL Multiphysics is illustrated in Fig. S3, with a channel width of 520 nm, channel length of 1500 nm, circular diameter of 20 nm, and spacing of 40 nm. To conserve computational resources, the model requires appropriate mesh generation. Given that the focus of this study is on the effect of the micro-column array on the gas-liquid interface in the bubble filtration process, the micro-column array region of the simulation model is finely meshed, while the remaining regions are meshed at a lower resolution. The meshing results are depicted in Fig. S4.
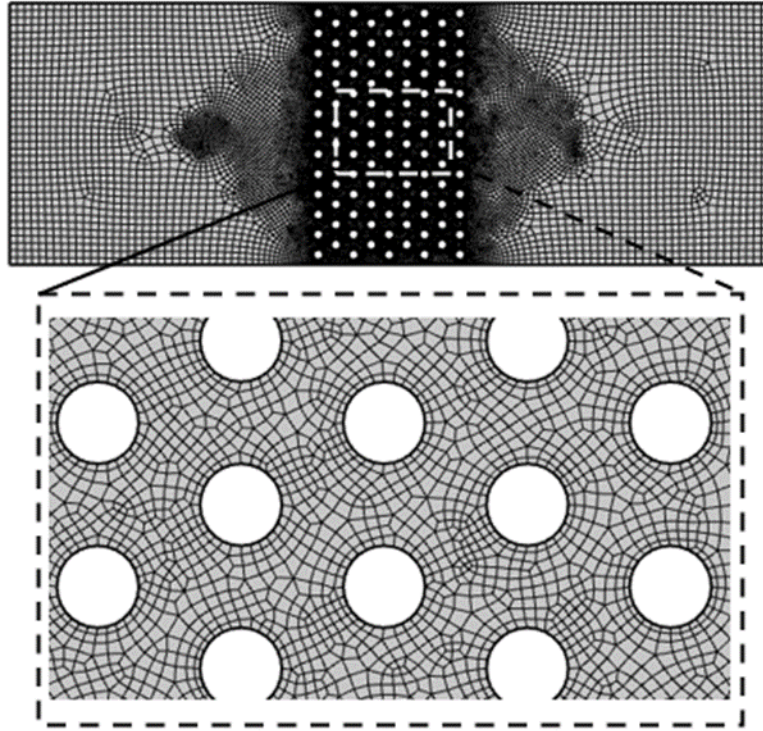
Fig. S4 Schematic diagram of meshing of computational model.

Simulation results and analysis.

To validate the mechanism of bubble filtration by stomatal pore membranes, this study conducted simulation and modeling of the process of bubble filtration through the stomatal membrane. This included investigating the influence of stomatal membrane surface wettability and maximum pore diameter on bubble filtration as well as the effect of stomatal membrane thickness on plant hydraulic transportation.

(1) Effect of surface wettability of pitted membrane on bubble filtration.

To examine the impact of stomatal membrane surface wettability on bubble filtration, the surface contact angles of the microcolumn array were set to 30° and 120°, respectively. The inlet pressure was set to 0.1 MPa. The process of bubble flow under different surface wettability conditions is illustrated in Fig.S5, where the blue region represents the liquid phase and the red region represents the gas phase. At a time of 900 μs, the gas phase failed to pass through the microcolumn array due to the action of surface tension, whereas under conditions with a wall contact angle of 120°, the gas phase successfully passed through the microcolumn array.
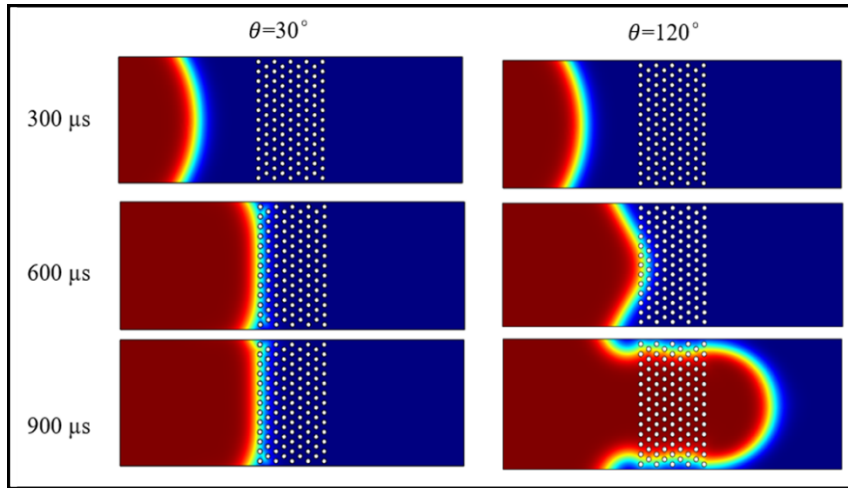
**Fig. S5 Effect of surface wettability on bubble filtration.**

Based on the simulation results, it is evident that surface wettability plays a crucial role in bubble filtration by stomatal membranes. The hydrophilicity of the stomatal membrane is a prerequisite for safe and effective bubble filtration. When the surface contact angle on the circular-shaped surface is 30°, and gradually increasing the inlet pressure until the gas phase passes through the microcolumn array results in a pressure of 6.4 MPa when the gas phase flows through, as shown in Fig. S6.
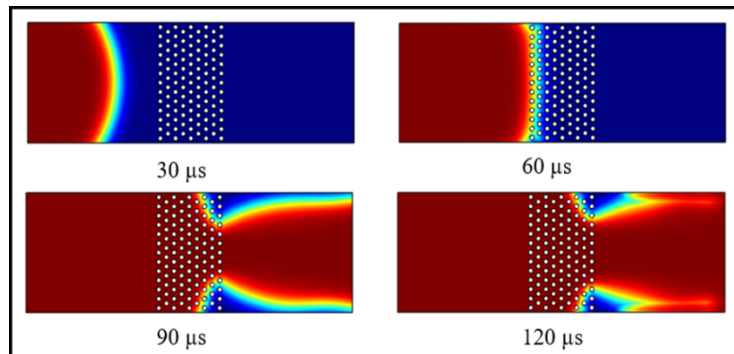
Fig. S6 Flow process of gas phase under 6.4MPa pressure.

(2) Effect of the maximum pore size of pitted membrane on bubble filtration.

The stomatal pore membrane has both average and maximum pore diameters. The average pore diameter is a crucial factor influencing the flow resistance of the stomatal membrane, whereas the maximum pore diameter affects the pressure when bubbles pass through the stomatal membrane. Smaller maximum pore diameters result in higher pressures when bubbles pass through. To investigate the relationship between the two, the gap sizes between microcolumn arrays were set to 70, 120, 170, and 220 nm for simulation, as shown in Fig. S6. In addition, the inlet pressure was gradually increased to obtain the pressure when gas passes through the microcolumn array. The simulation results and theoretical calculations of the gas leakage threshold for different pore sizes and their relationship with the gap size between microcolumns are illustrated in Fig. S7. The results indicate that the gas leakage threshold is inversely proportional to the pore size of circular-shaped gaps.
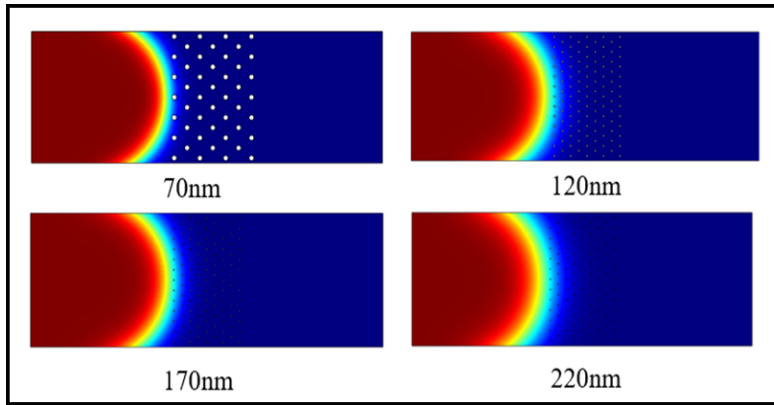
Fig. S7. Simulation results of models with pore sizes of 70nm, 120nm, 170nm and 220nm.

According to the simulation results, the ability of the stomatal membrane to filter bubbles is determined by the maximum pore diameter of the membrane. The smaller the maximum pore diameter of the stomatal membrane, the higher the gas leakage threshold. Previous studies[1-3] have shown that thicker stomatal membranes have smaller average pore diameters and smaller maximum pore diameters, resulting in higher gas leakage thresholds and stronger resistance to blockage. Thicker stomatal membranes are mechanically more robust which lead to greater tensile resistance and prevent pore enlargement. Thicker stomatal membranes have higher gas leakage thresholds; however, they also have higher flow resistance. Therefore, it is necessary to conduct simulation analysis on the effect of stomatal membrane thickness on fluid flow rate.

(3) Effect of pitted film thickness on fluid flow.

Using a porous media model to investigate the effect of stomatal membrane thickness on fluid flow. The simulation model, as shown in Fig. S8(a), consists of three regions, with the middle region being the porous media area. The simulation results, illustrated in Fig. S8(c) and Fig. S8(d), show that during fluid flow, the majority of the pressure is used to overcome the resistance of the porous media, resulting in a significant pressure difference on either side of the porous media. Simulations were conducted for models with porous media domain widths ranging from 100 to 1300 nm and the mass flow rate of the liquid at 0.1 MPa pressure is depicted in Fig. S8(b). The simulation results indicate that as the stomatal membrane thickness increases, the resistance to fluid flow also increases, leading to a decrease in fluid mass flow rate.
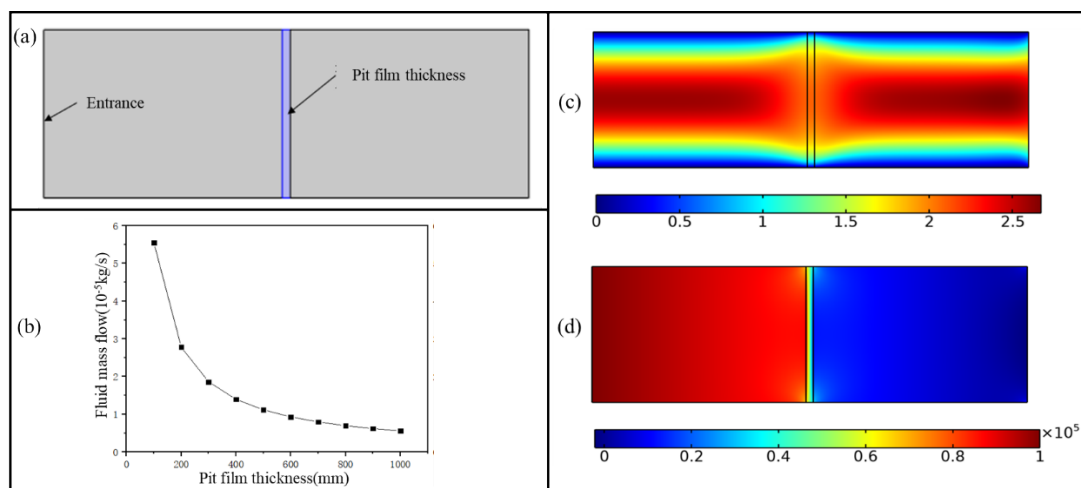
Fig. S8 Simulation results of the influence of pitted film thickness on fluid flow. (a) Division of the simulation model of the influence of pitted film thickness on fluid flow. (b) Relationship between pitted film thickness and fluid mass flow. (c) Effect of pitted film thickness on fluid flow simulation velocity cloud map, m/s. (d) Effect of pitted film thickness on fluid flow simulation pressure cloud map, Pa.

The cellulose is crosslinked with polyvinyl alcohol (PVA) to produce hydrogel.

In order to create biomimetic microstructures capable of filtering bubbles, hydrogel is introduced to form biomimetic pore membranes within the microstructures, aiming to achieve bubble filtration. When selecting hydrogel, the following principles should be considered: (1) the hydrogel should be hydrophilic; (2) the crosslinking speed of the hydrogel should be controllable, and the initial solution viscosity should be low; (3) the crosslinking environment should be simple and easy to operate; (4) no toxic substances should be generated during the crosslinking process.

Plant stomatal pores are mainly composed of cellulose. In this study, cellulose-based hydrogel is used as the material for biomimetic pore membranes to mimic the hydrophilic properties of stomatal pores and enable the microstructures to filter bubbles. Cellulose, as a naturally abundant renewable polymer material, possesses characteristics such as renewability, low cost, biocompatibility and biodegradability which render it an ideal material for preparing hydrogels[4-6].

Due to the presence of intramolecular and intermolecular hydrogen bonding interactions, the chemical structure of cellulose is stable and typically difficult to dissolve directly in water and organic solvents. Currently, there are four solvent systems for dissolving cellulose: dimethylacetamide/ lithium chloride (DMAC/LiCl) system, ionic liquid system, N-methylmorpholine-N-oxide (NMMO) system, and alkali/urea system. In these systems, cellulose is dissolved by utilizing the anions in the solution to disrupt the original hydrogen bonds in the cellulose molecules and form new hydrogen bonds, resulting in cellulose dissolution. In the alkali/urea solution system, sodium hydroxide and urea first form hydrogen bonds, and then interact with the cellulose chains to dissolve cellulose quickly. Moreover, the alkali/urea (or thiourea) aqueous system is a cheap, non-polluting novel cellulose solvent which is the fastest cellulose

dissolution rate among non-derivatized aqueous systems and has a longer storage period.

The preparation of hydrogels involves crosslinking polymer materials to form a three-dimensional network structure. There are two types of crosslinking methods: physical crosslinking and chemical crosslinking. Physical crosslinking refers to treating cellulose through physical methods such as heating, freezing, stirring, ultrasound, etc., to form hydrogels by crosslinking molecules through hydrogen bonds, van der Waals forces, and coordination bonds. Chemical crosslinking involves adding crosslinking agents to the system, and crosslinking is achieved through chemical bonds formed between the crosslinking agent and cellulose.
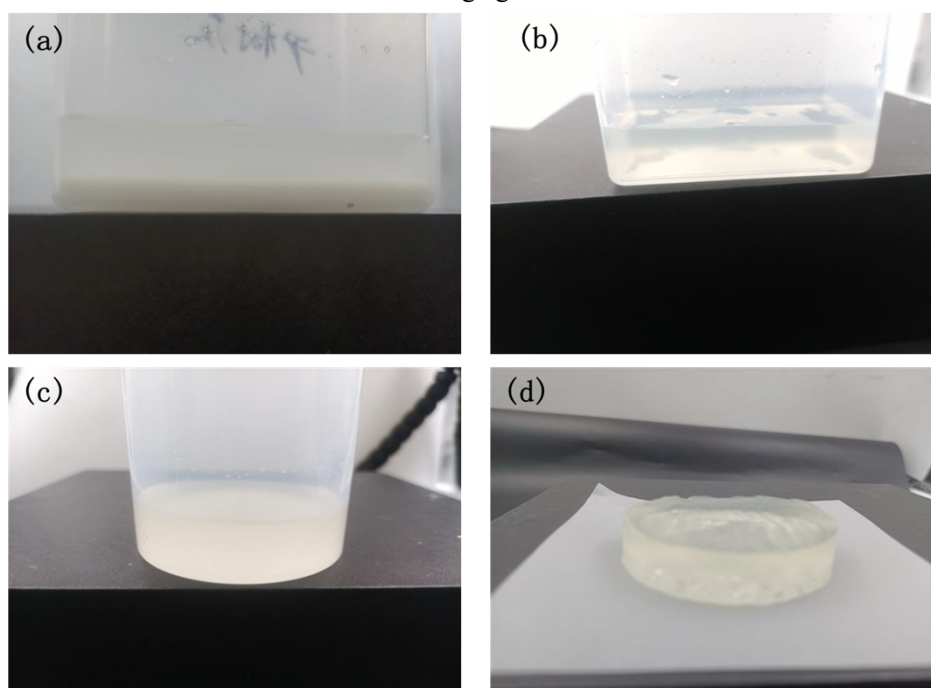
Fig.S9 Fabrication of cellulose/PVA hydrogels.

Polyvinyl alcohol (PVA) is a water-soluble polymer with biocompatibility. It has been synthesized into hydrogels using both chemical crosslinking methods (radiation treatment) and physical methods (freeze/thaw cycles). The crosslinking speed of cellulose/PVA hydrogels is controllable, and their initial solution viscosity is low, making them suitable for the formation of biomimetic pore membranes. Therefore, in this study, cellulose and polyvinyl alcohol (PVA) were crosslinked to produce hydrogels. The process of preparing and testing cellulose/PVA hydrogels is as follows:

(1) Preparation of Cellulose/PVA Hydrogels

①Disperse 4 g of cellulose into a mixture solution of 96 g of sodium hydroxide, urea, and water (V:V:V=6:4:90). As shown in Fig. S9 (a), cellulose is insoluble in the aqueous solution at room temperature. After adding cellulose to the mixture solution and stirring, the cellulose and the mixture solution separate into layers upon standing. After thorough stirring, the mixture is placed at -20 °C for 12 hours for cold dissolution, followed by thawing at room temperature to obtain a 4% cellulose solution, as shown in Fig. S9 (b).

②Dissolve PVA in the same solvent to obtain a 4% PVA solution, as shown in Fig. S9 (c).

③Mix the cellulose solution and PVA solution in a 1:1 ratio, then add the crosslinking agent, epichlorohydrin (ECH). Stir the mixture at 30 °C for 30 minutes, then crosslink at 60 °C for 6 hours to obtain the cellulose/PVA hydrogel, as shown in Fig. S9 (d).

(2) Contact Angle Measurement of Cellulose/PVA Hydrogel

After the preparation of the cellulose/PVA hydrogel, the contact angle of the gel was measured using a contact angle measurement device. Multiple measurements were taken at different positions on the hydrogel, and the average contact angle was calculated to be 35.5°, as shown in Fig. S10.
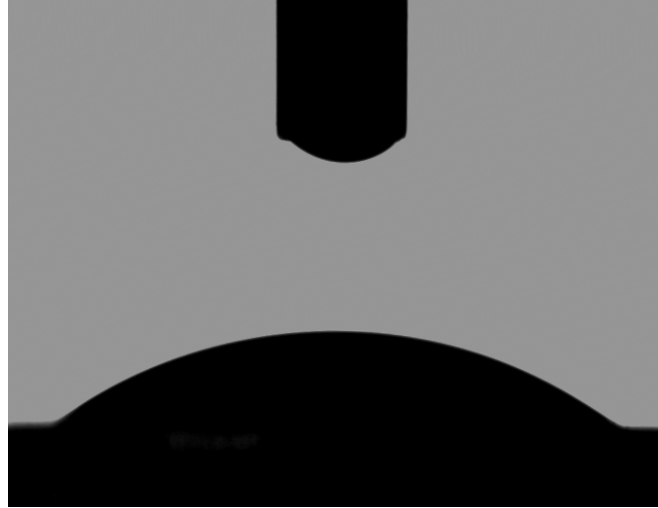
Fig.S10 Contact angle of cellulose/PVA hydrogel.

(3) Viscosity Variation of Cellulose/PVA Hydrogel during Preparation

To monitor the viscosity variation of the cellulose/PVA hydrogel during preparation, viscosity measurements were conducted every 10 minutes using a rheometer after thorough mixing of cellulose and PVA solution with the addition of crosslinking agent for 30 minutes. The viscosity results are illustrated in Fig. S11. Within the first hour after mixing the gel solution, the viscosity change was relatively slow. However, after an hour, the viscosity of the solution increased significantly over time, exceeding 21,000 mPa.s after 2 hours. Based on the trend of viscosity change in the gel solution over time, the optimal time for injecting the hydrogel into the microstructure unit channels to create biomimetic pore membranes is within the first hour after thorough and uniform mixing of the gel solution.
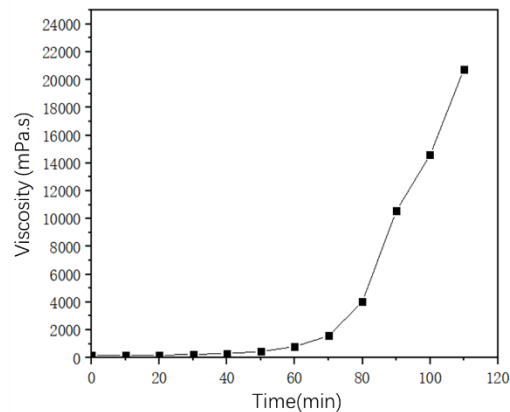
Fig.S11 Variation of gel solution viscosity with time.

Based on the surface wettability and viscosity measurements of the cellulose/PVA hydrogel, it can be concluded that the hydrogel is suitable as a material for biomimetic pore membranes.

The experimental chips were fabricated using the casting molding method.

Polydimethylsiloxane (PDMS), also known as silicone rubber, is a typical thermosetting material characterized by excellent transparency, permeability and chemical inertness[7]. It is processed easily with simple molding techniques and can undergo reversible and repetitive deformation without permanent damage. Therefore, PDMS is chosen as the substrate material for the experimental microstructure unit chips in this study.

Various methods are available for the fabrication of microfluidic chips, including hot embossing, casting molding, and injection molding. Hot embossing involves replicating the structures from a mold onto the material under high temperature and pressure. Injection molding entails pouring molten material into a mold containing the desired structures and allowing it to cool and solidify. Casting molding involves pouring material onto a mold and then demolding after solidification to replicate the structures.

In this study, PDMS is used as the material for the experimental chips, and the casting molding method is employed for chip fabrication. The fabrication process includes mask design, mold fabrication, casting molding and chip bonding. Considering factors such as structural accuracy, production cycle, and cost, molds are fabricated using negative SU-8 material, and the fabrication process is conducted in a cleanroom laboratory. The fabrication process is illustrated in Fig. S12.

①Select a 10×10 cm glass slide as the mold substrate, wipe it with acetone to remove any residual impurities, and pre-bake it on a hot plate at 85°C for 10 minutes to eliminate residual acetone.

②Spin-coat a layer of BN303 on the glass slide using a spin coater to enhance the adhesion between glass and SU-8. Post-bake the coated glass slide on an 85°C hot plate for 20 minutes. Spin-coating parameters: low speed for 9 seconds at 600 rpm, high speed for 30 seconds at 2500 rpm. After the post-bake, expose the BN303 layer to full UV light in a lithography machine to cure and form an intermediate adhesive layer.

③Apply a layer of negative SU-8 resist onto the fully exposed glass slide and ensure uniform distribution by tilting the glass. Place the glass slide in a spin coater to form the SU-8 layer. Spin-coating parameters: low speed for 9 seconds at 600 rpm, high speed for 30 seconds at 1200 rpm. After spin-coating, allow the SU-8 layer to stand for 20 minutes and then post-bake at 85°C for 30 minutes.

④After the post-bake, perform incomplete exposure on the SU-8 layer using a mask. The exposed SU-8 areas will quickly crosslink and solidify upon absorption of light energy, while the unexposed areas will be removed through development.

⑤Post-bake the partially exposed SU-8 layer on an 85°C hot plate for 2.5 minutes.

⑥Develop the SU-8 mold by immersing it in a developer solution. After 2 minutes, confirm completion of development by observing the flow of liquid on the mold surface. Rinse the developed mold with deionized water and dry it with nitrogen gas.

⑦Silanize the mold by placing it in a desiccator, dripping 0.8 ml of trimethylchlorosilane for sealing, and smoking it for 20 minutes to facilitate demolding after PDMS casting
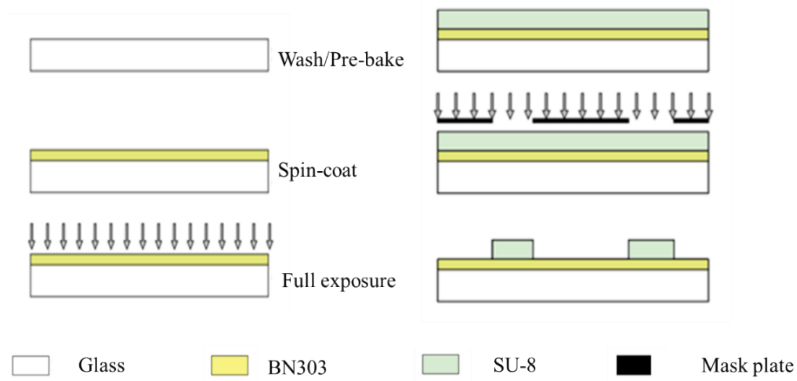
Fig.S12 SU-8 mold making process.

Once the mold fabrication is complete, measure the height (channel depth) of the microstructures on the mold using a stylus profilometer. The designed mold height is 30 μm, and multiple points are measured with an error range of 0.31μm to 0.89 μm.

For the fabrication of biomimetic microfluidic chips using injection molding, follow the steps outlined below:

①Wrap the silanized SU-8 mold with aluminum foil and use compressed air to remove any impurities from the mold surface.

②Mix PDMS prepolymer and curing agent at a ratio of 10:1, thoroughly stir the mixture, and inject it onto the mold using a syringe. Remove air bubbles from the PDMS using a vacuum oven. Subsequently, cure the PDMS in a nitrogen oven at 85°C for 2 hours.

③Demold the cured PDMS and punch holes if necessary. Treat the surface using a plasma cleaner and complete the chip bonding process.

References:

1.   Zhang, Y.; Carmesin, C.; Kaack, L.; Klepsch, M. M.; Kotowska, M.; Matei, T.; Schenk, H. J.; Weber, M.; Walther, P.; Schmidt, V.; Jansen, S., High porosity with tiny pore constrictions and unbending pathways characterize the 3D structure of intervessel pit membranes in angiosperm xylem. *PLANT CELL AND ENVIRONMENT* **2020,** 43, (1), 116-130.

2.   Kaack, L.; Weber, M.; Isasa, E.; Karimi, Z.; Li, S.; Pereira, L.; Trabi, C. L.; Zhang, Y.; Schenk, H. J.; Schuldt, B.; Schmidt, V.; Jansen, S., Pore constrictions in intervessel pit membranes provide a mechanistic explanation for xylem embolism resistance in angiosperms. *NEW PHYTOLOGIST* **2021,** 230, (5), 1829-1843.

3.   Schmitz, N.; Koch, G.; Beeckman, H.; Koedam, N.; Robert, E. M. R.; Schmitt, U., A STRUCTURAL AND COMPOSITIONAL ANALYSIS OF INTERVESSEL PIT MEMBRANES IN THE SAPWOOD OF SOME MANGROVE WOODS. *IAWA JOURNAL* **2012,** 33, (3), 243-256.

4.   Parhi, R., Cross-Linked Hydrogel for Pharmaceutical Applications: A Review. *Adv Pharm Bull* **2017,** 7, (4), 515-530.

5.   Ahmed, E. M., Hydrogel: Preparation, characterization, and applications: A review. *JOURNAL OF ADVANCED RESEARCH* **2015,** 6, (2), 105-121.

6.   Simon, J.; Muller, H. P.; Koch, R.; Muller, V., Thermoplastic and biodegradable polymers of cellulose. *POLYMER DEGRADATION AND STABILITY* **1998,** 59, (1-3), 107-115.

7.   Yadhuraj, S. R.; Gandla, S. B.; Sudarshan, B. G.; Kumar, P. S. C., Preparation and Study of PDMS Material. *MATERIALS TODAY-PROCEEDINGS* **2018,** 5, (10), 21406-21412.